JASMAC
Conference of the Japan Society of Microgravity Application

OR3-7

格子ボルツマン法とフェーズフィールド法による相変化解析手法の開発

Development of phase change simulation method by Lattice Boltzmann Method and Phase Field Method

小島岬 [1], 田川俊夫 [1]
Misaki KOJIMA[1], Toshio TAGAWA[1]
1 東京都立大学航空宇宙システム工学域, Department of Aeronautics and Astronautics, Tokyo Metropolitan University

1. Introduction

Gas-liquid two-phase flows including phase changes are used in various industrial devices such as combustion engines, boilers, heat exchangers, and nuclear reactors. Therefore, accurate prediction of gas-liquid two-phase flows is necessary to improve the performance of such devices. However, due to the high complexity and small time and space scales of this phenomenon, complete prediction of this phenomenon by experiments is often difficult. Therefore, prediction and understanding of this phenomenon by numerical simulation is important.

Different numerical simulation methods have been presented to predict gas-liquid two-phase flows including phase changes. The most common methods are the Volume of Fluid (VOF) method[1)], the Level-Set method[2,3)], and the Front-Tracking method[4)]. In recent years, the Lattice Boltzmann Method (LBM)[5,6)] has been attracting attention as an alternative to these methods. The LBM is the numerical method to simulate a macroscopic flow field by representing a fluid by a set of virtual particles and calculating the streaming and collision of these virtual particles using distribution functions. The LBM has the following features[7)]: high parallel computing performance due to its fully explicit method and local memory access, high conservation properties due to its fully advective, and ability to treat complex phenomena and boundaries. Due to these features, the LBM is expected to be applied to gas-liquid two-phase flows. However, when the LBM is used to simulate the gas-liquid two-phase flows, the calculation at high density ratio tends to be unstable. Therefore, different improvements have been presented to simulate the high density ratio two-phase flows[8-14)]. Currently, simulations with a density ratio around 1000 are possible by the LBM. Similarly, when considering phase changes in gas-liquid two-phase flows by the LBM, numerical stability at high density ratio is a problem.

When simulating gas-liquid two-phase flows including phase changes by the LBM, the pseudopotential LBM which expresses the gas-liquid interface by introducing a pseudopotential between particles is often used[15)]. On the other hand, the Phase Field LBM has been attracting attention for phase change simulations in the viewpoint of adaptation to high density ratio and thermodynamic consistency[16-18)]. In the Phase Field LBM, the gas-liquid interface is modeled as the finite volume region on a system of fixed grids where properties change continuously and rapidly, and the interface shape is determined autonomously by solving the Chan-Hilliard (C-H) equation or Allen-Cahn (A-C) equation which are based on free energy theory. This method is considered to be able to simulate the phase change of the high-density ratio. However, the validation of this method at high density ratios is limited to the one-dimensional Stefan problems and the droplet evaporation problems in which interface deformation is almost zero. Hence, the purpose of this study is to develop a simulation method for two-phase flows including phase changes with large interface deformations, based on velocity-based Phase Field LBM[14,18)], which is considered to have high numerical stability at high density ratios among Phase Field LBMs.

2. Numerical method

2.1 Macroscopic equation

In this study, one-component, incompressible in each phase, the compressibility due to the phase change at the interface is modeled as a source term[16)], gas-liquid two-phase flow is considered. The macroscopic equations are the conservation of mass (1), the conservation of momentum (2), the conservation of energy (3), and the Conservative-Allen-

Cahn(C-A-C) equation (4), which determines the interface profile by minimizing the total free energy of the system. The C-H equation is usually used in the simulations of gas-liquid two-phase flows by the Phase Field Method. In recent years, however, it has been proposed to use the C-A-C equation in which the effect of the curvature is removed from A-C equation, and the equation is transformed into the conservative form [19-21]. The C-H equation is a fourth-order partial differential equation, while the C-A-C equation is a second-order partial differential equation. Therefore, it is said that the C-A-C equation enables more accurate analysis than the C-H equation. Hence, the C-A-C equation is adopted as the governing equation in this study. The liquid phase temperature is fixed at saturation and energy equation is solved only in the gas phase[16]. The macroscopic equations are

$$\frac{\partial u_\alpha}{\partial x_\alpha} = \dot{m}'''\left(\frac{1}{\rho_l} - \frac{1}{\rho_h}\right) \tag{1}$$

$$\rho\left(\frac{\partial u_\alpha}{\partial t} + u_\beta \frac{\partial u_\alpha}{\partial x_\beta}\right) = -\frac{\partial p}{\partial x_\alpha} + \frac{\partial \tau_{\alpha\beta}}{\partial x_\beta} + F_\alpha^s + F_\alpha^b \tag{2}$$

$$\rho_l c_{pl}\left(\frac{\partial T}{\partial t} + u_\alpha \frac{\partial T}{\partial x_\alpha}\right) = \frac{\partial}{\partial x_\alpha}\left(\lambda_l \frac{\partial T}{\partial x_\alpha}\right) \tag{3}$$

$$\frac{\partial \phi}{\partial t} + \frac{\partial \phi u_\alpha}{\partial x_\alpha} = \frac{\partial}{\partial x_\alpha} M\left[\frac{\partial \phi}{\partial x_\alpha} - \frac{\partial \phi}{\partial x_\alpha}\Big/\left|\frac{\partial \phi}{\partial x_\beta}\right|\left[\frac{1-4(\phi-0.5)^2}{W}\right]\right] - \frac{\dot{m}'''}{\rho_h} \tag{4}$$

where ϕ is the order parameter that indicates each phase, i.e. $\phi = 1$ indicates liquid phase, $\phi = 0$ indicates gas phase, and $0 < \phi < 1$ indicate interface. Besides, u_α is the velocity, ρ is the density, p is the pressure, $\tau_{\alpha\beta}$ is the viscous stress, T is the temperature, c_p is the specific heat, λ is the thermal conductivity, M is the mobility, W is the interface thickness, $\dot{m}'''$ is the amount of phase change per unit time unit volume, F_α^s is the surface tension force, and F_α^b is the body force. The suffix h and l indicates heavy and light fluids and the suffix α and β follows Einstein's summation convention. The surface tension force F_α^s is modeled by the following potential form and the amount of phase change $\dot{m}'''$ is modeled based on the energy balance for the interface regions[16]:

$$F_\alpha^s = \eta \frac{\partial \phi}{\partial x_\alpha} \tag{5}$$

$$\dot{m}''' = -\frac{\lambda_h}{L}\frac{\partial T}{\partial x_\alpha}\frac{\partial \phi}{\partial x_\alpha} \tag{6}$$

where L is the latent heat and η is the chemical potential defined as

$$\eta = 4\beta_\phi \phi(\phi-1)(\phi-0.5) - k_\phi \frac{\partial^2 \phi}{\partial x_\alpha \partial x_\alpha} \tag{7}$$

where k_ϕ and β_ϕ are coefficients related to the interface thickness W and surface tension coefficient σ, and are given by $k_\phi = 3\sigma W/2$ and $\beta_\phi = 12\sigma/W$. In this study, the Mach number and temperature changes are assumed to be small, and the physical properties in each phase are treated as constants. The density and the viscosity are given by $\psi = \psi_l + \phi(\psi_h - \psi_l)$ using the order parameter, where $\psi = (\rho, \mu)$.

2.2 Lattice Boltzmann method

In this study, two distribution functions, g_i for analyzing the equations (1) and (2) and h_i for analyzing the equation (4), are introduced and numerical simulations are conducted by solving the time evolution equations for each of them. The time evolution equations for g_i is based on velocity-based-LBM[14,18], which is considered to achieve high numerical stability and computational efficiency. Moreover, additional forcing term and the source term are derived to recover the macroscopic equations (1) and (2) by the Chapman-Enskog theory and added to the time evolution equations. The time evolution equations for h_i is based on the method of Geier et al[21], and added the source term to recover the macroscopic equation (4). The energy equation is discretized and solved by the Euler method and the second-order central difference. The time evolution equations for the distribution functions are given by

$$g_i(x_\alpha + c_{i\alpha}\Delta t, t + \Delta t) = g_i(x_\alpha, t) + \Omega_i^g + F_i + Q_i^g \tag{8}$$

$$h_i(x_\alpha + c_{i\alpha}\Delta t, t + \Delta t) = h_i(x_\alpha, t) + \Omega_i^h + Q_i^h \tag{9}$$

where Q_i^g and Q_i^h are the source terms in the LBM, F_i is the forcing term in the LBM, and Ω_i^g and Ω_i^h are the collision terms. In the LBM, the collision term is modeled by various ways. The most basic one is the Single Relaxation Time (SRT) model. In the SRT model, all distribution functions are assumed to reach equilibrium at the same time. Therefore, the SRT model is simple, but the numerical stability is low. The Multi Relaxation Time (MRT) model[6,22] is modified version of the

SRT model. In the MRT model, distribution functions are transformed into macroscopic physical quantities, and different relaxation coefficients are applied to each physical quantity. Therefore, the numerical stability and accuracy is increased by the MRT model. Hence, in this study, the MRT model is applied to the collision term. The source terms in the LBM, the forcing term in the LBM, and the collision terms are given by

$$\Omega_i^g = -\boldsymbol{N^{-1}S^g N}(g - g^{eq}) \tag{10}$$

$$\Omega_i^h = -\boldsymbol{N^{-1}S^h N}(h - h^{eq}) \tag{11}$$

$$F_i = \Delta t w_i \frac{c_{i\alpha}F_\alpha}{\rho c_s^2}, F_\alpha = F_\alpha^s + F_\alpha^b + F_\alpha^\mu + F_\alpha^p + F_\alpha^a \tag{12}$$

$$Q_i^g = \Delta t w_i \dot{m}''' \left(\frac{1}{\rho_l} - \frac{1}{\rho_h}\right) \tag{13}$$

$$Q_i^h = -\Delta t w_i \frac{\dot{m}'''}{\rho_h} \tag{14}$$

where $\boldsymbol{N}$ is the transformation matrix to transform the distribution functions into the macroscopic physical quantities, $\boldsymbol{S^g}$ and $\boldsymbol{S^h}$ are the following diagonal matrices including the relaxation coefficients applied to each physical quantity, g^{eq} and h^{eq} are the following equilibrium distribution functions, and F_α^μ, F_α^p, and F_α^a are the following forcing term required to recover equations (1) and (2) by the Chapman-Enskog theory:

$$\boldsymbol{S^g} = \mathrm{diag}\big(1,1,1,1,1,1,s_g,s_g\big), s_g = \frac{1}{\tau_g + 0.5}, \mu = \rho\tau_g c_s^2 \tag{15}$$

$$\boldsymbol{S^h} = \mathrm{diag}(0,1.5,1.5,s_h,1.5,s_h,1.5,1.5,1.5), s_h = \frac{1}{\tau_h + 0.5}, M = \tau_h c_s^2 \Delta t \tag{16}$$

$$g_i^{eq} = p^* w_i + (\Gamma_i - w_i) - \frac{1}{2}F_i, \Gamma_i = w_i\left[1 + \frac{c_{i\alpha}u_\alpha}{c_s^2} + \frac{(c_{i\alpha}u_\alpha)^2}{2c_s^4} - \frac{u_\alpha^2}{2c_s^2}\right], p^* = \frac{p}{\rho c_s^2} \tag{17}$$

$$h_i^{eq} = \phi\Gamma_i + \frac{M}{c_s^2}\left[\frac{1 - 4(\phi - 0.5)^2}{W}\right] w_i c_{i\alpha}\frac{\partial\phi}{\partial x_\alpha} \Big/ \left|\frac{\partial\phi}{\partial x_\beta}\right| - \frac{1}{2}Q_i^h \tag{18}$$

$$F_\alpha^\mu = \frac{\mu}{\rho}\left(\frac{\partial u_\beta}{\partial x_\alpha} + \frac{\partial u_\alpha}{\partial x_\beta}\right)\frac{\partial\rho}{\partial x_\beta} = -\frac{\mu}{\rho c_s^2 \Delta t}\left[\sum_j c_{j\alpha}c_{j\beta}\sum_i (\boldsymbol{N^{-1}SN})_{ji}\big(g_i - g_i^{eq}\big)\right]\frac{\partial\rho}{\partial x_\beta} \tag{19}$$

$$F_\alpha^p = -c_s^2 p^* \frac{\partial\rho}{\partial x_\alpha} \tag{20}$$

$$F_\alpha^a = \rho u_\alpha \frac{\partial u_\beta}{\partial x_\beta} \tag{21}$$

where w_i is the weight coefficient, $c_{i\alpha}$ is the discrete velocity, c_s is the speed of sound in the system, and i is the discrete velocity number. In this study, we use the D2Q9 model and w_i, $c_{i\alpha}$ and c_s are defined as

$$c_{i\alpha} = c\begin{cases} (0,0) & i = 0 \\ (\pm1,0),(0,\pm1) & i = 1\sim4 \\ (\pm1,\pm1) & i = 5\sim8 \end{cases}, w_i = \begin{cases} 4/9 & i = 0 \\ 1/9 & i = 1\sim4 \\ 1/36 & i = 5\sim8 \end{cases}, c_s = \frac{c}{\sqrt{3}}, c = \frac{\Delta x}{\Delta t} = 1 \tag{22}$$

In the LBM, the macroscopic physical quantities are obtained by taking the moment of the distribution functions:

$$\phi = \sum_i h_i + \frac{1}{2}\sum_i Q_i \tag{23}$$

$$p^* = \sum_i g_i \tag{24}$$

$$u_\alpha = \sum_i c_{i\alpha} g_i + \frac{F_\alpha \Delta t}{2\rho} \tag{25}$$

The gradient of the density in equations (19) and (20) is computed by

$$\frac{\partial \rho}{\partial x_\alpha} = (\rho_h - \rho_l)\frac{\partial \phi}{\partial x_\alpha} \tag{26}$$

The way to compute the gradient of the order parameter in equations (5), (6), (18), and (26) is important for the stability of the high density ratio. Therefore, in this study, the gradient of the order parameter is computed by the following weighting of the second-order isotropic finite difference method and the third-order isotropic finite difference method[22,23]:

$$\frac{\partial \phi}{\partial x_\alpha} = (1-Z)\frac{\overline{\partial \phi}}{\partial x_\alpha} + Z\frac{\overline{\overline{\partial \phi}}}{\partial x_\alpha}, Z = \frac{1}{3} \tag{27}$$

$$\frac{\overline{\partial \phi}}{\partial x_\alpha} = \frac{c}{c_s^2 \Delta x}\sum_i c_{i\alpha} w_i \phi(x_i + c_{i\alpha}\Delta t, t) \tag{28}$$

$$\frac{\overline{\overline{\partial \phi}}}{\partial x_\alpha} = \frac{c}{c_s^2 \Delta x}\sum_i c_{i\alpha} w_i \frac{4\phi(x_i + c_{i\alpha}\Delta t, t) - \phi(x_i + 2c_{i\alpha}\Delta t, t)}{2} \tag{29}$$

2.3 Initial condition and Boundary condition

The initial conditions for the distribution functions are given by the equilibrium distribution functions (17) and (18) using the initial conditions for macroscopic physical quantities. The initial condition for the interface profile is given by the equilibrium solution of C-A-C equation:

$$\phi = \frac{1}{2} + \frac{1}{2}\tanh\left(\frac{2s}{W}\right) \tag{30}$$

where s is the signed distance function of the interface located at $s = 0$.

The unknown distribution functions on the boundary need to be given as boundary conditions. For the no-slip boundary condition, the Bounce-Back condition is used to obtain the unknown distribution functions on the boundary. For the periodic boundary condition, the distribution functions that flow out from the opposite boundary are used to obtain the unknown distribution functions on the boundary. For the outlet boundary condition, the equilibrium distribution functions obtained from the macroscopic physical quantities on the boundary are used to obtain the distribution functions in all directions on the boundary.

All physical variables used in this study are made dimensionless using characteristic length L_0, characteristic particle speed c_0, reference fluid density ρ_0, reference temperature T_0, reference specific heat c_{p0}, and characteristic time scale $t_0 = L_0/c_0$. In this study, L_0 is taken as the lattice width.

3. Results and discussions

3.1 Stefan problem

The validity of the phase change model and employing the C-A-C equation to phase change simulations is verified by the Stefan problem[2] for which an analytical solution exists. Fig. 1 shows the computational model. As an initial condition, a thin vapor phase is placed next to the heating wall at the temperature T_w which is slightly higher than the saturation temperature, and a liquid phase at the saturation temperature T_{sat} is placed next to it. As times passes, the energy which is transferred from the heating wall to the vapor phase causes a phase change, and the vapor phase region expands. In this process, the densities of the vapor phase and the liquid phase are assumed to be equal, and each of the vapor phase and liquid phase can be regarded as stationary. Therefore, in this study, the validity of the phase change model and employing the C-A-C equation to phase change simulations is verified by assuming equal density and neglecting the fluid field. Table 1 shows the computational conditions.

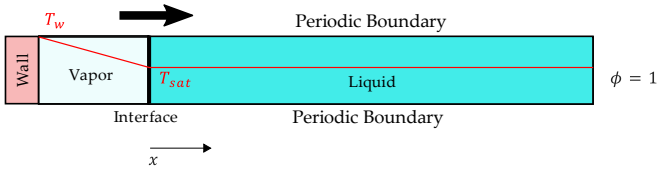

Fig. 1 Computational model for Stefan problem

Table 1 Computational conditions for Stefan problem

Parameter	Symbol	Value
Specific heat ratio	c_{ph}/c_{pl}	1.0
Thermal conductivity ratio	λ_h/λ_l	2.0
Stefan number	St	1.0/0.5/0.1
Grids	$L_x \times L_y$	128×16

where Stefan number St is the dimensionless number defined as

$$St = \frac{c_{ph}(T_w - T_{sat})}{L} \tag{31}$$

The analytical solution for the interface position x_{if} is given by solving the heat conduction equation for the vapor phase under the moving boundary condition using the similarity transformation:

$$x_{if} = 2\xi_{if}\sqrt{\frac{\lambda_l}{\rho_l c_{pl}}t}\,, \xi_{if}\,\mathrm{erf}(\xi_{if})\,e^{\xi_{if}^2} = c_{pl}\frac{T_w - T_{sat}}{L\sqrt{\pi}} \tag{32}$$

Fig. 2 shows comparison between the analytical solution and the simulation results by the present method for the evolution of liquid-vapor interface location. The simulation results agree well with the analytical solution. Therefore, the phase change model and employing the C-A-C equation to phase change simulations is valid.

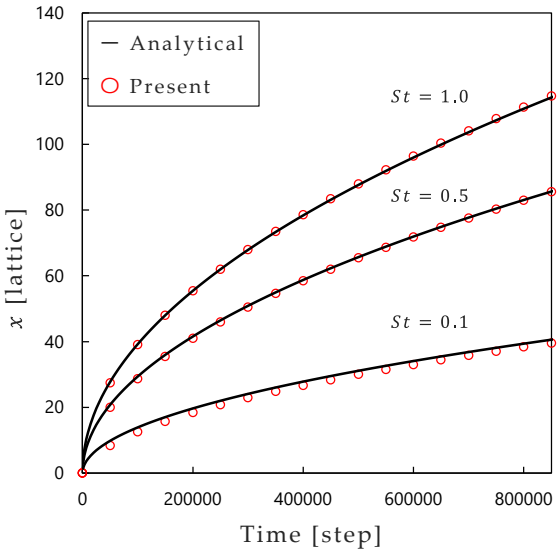

Fig. 2 Evolution of the liquid-vapor interface location for Stefan problem. The lines indicate analytical solutions by Eq. (32) and the dots indicate present numerical results for each Stefan number.

3.2 Droplet evaporation

The validity of the method to simulate the flow field by the LBM is verified by the droplet evaporation problem[24] for which an analytical solution exists. Fig. 3 shows the computational model. As an initial condition, a droplet at the saturation temperature T_{sat} is placed at the center of the computational domain and surrounded by a vapor phase at the temperature T_w which is slightly higher than the saturation temperature. A droplet size change due to the phase change at the interface is simulated. To ensure symmetry, the computational domain is divided into four parts, and one of these regions is simulated using the symmetric boundary condition. In addition, at the outlet boundary, the temperature is given as T_w, the pressure is given as zero, and the normal gradients of velocities and order parameter are given as zero. Table 2 shows the computational conditions.

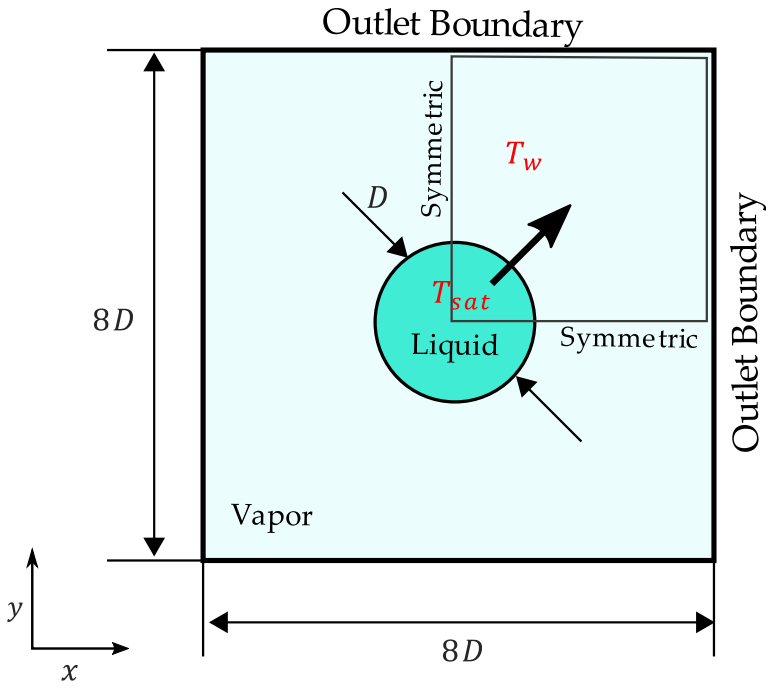

Fig. 3 Computational model for Droplet evaporation

Table 2 Computational conditions for Droplet evaporation

Parameter	Symbol	Value
Density ratio	ρ_h/ρ_l	1000 / 100
Viscosity ratio	μ_h/μ_l	10
Specific heat ratio	c_{ph}/c_{pl}	1.0
Thermal conductivity ratio	λ_h/λ_l	10
Stefan number	St	0.1
Laplace number	La	10000
Prandtl number	Pr	1.0
Grids	$4D \times 4D$	128×128

where Laplace number La and Prandtl number Pr are the dimensionless numbers defined as

$$La = \frac{\sigma \rho_h D}{\mu_h^2} \tag{33}$$

$$Pr = \frac{\mu_h c_{ph}}{\lambda_h} \tag{34}$$

The analytical solution for the droplet diameter is given by following d^2-law[24]:

$$\frac{dd_r^2}{dt} = -\frac{8\lambda_l}{\rho_h c_{pl}} \frac{\ln\left(1 + c_{pl}(T_w - T_{sat})/L\right)}{\ln(8D/d_r)} \tag{35}$$

where d_r is the droplet diameter. Fig. 4 shows comparison between the analytical solution and the simulation results by the present method for the evolution of droplet diameter. The simulation results agree well with the analytical solution. Therefore, the method to simulate the fluid field by the LBM is valid.

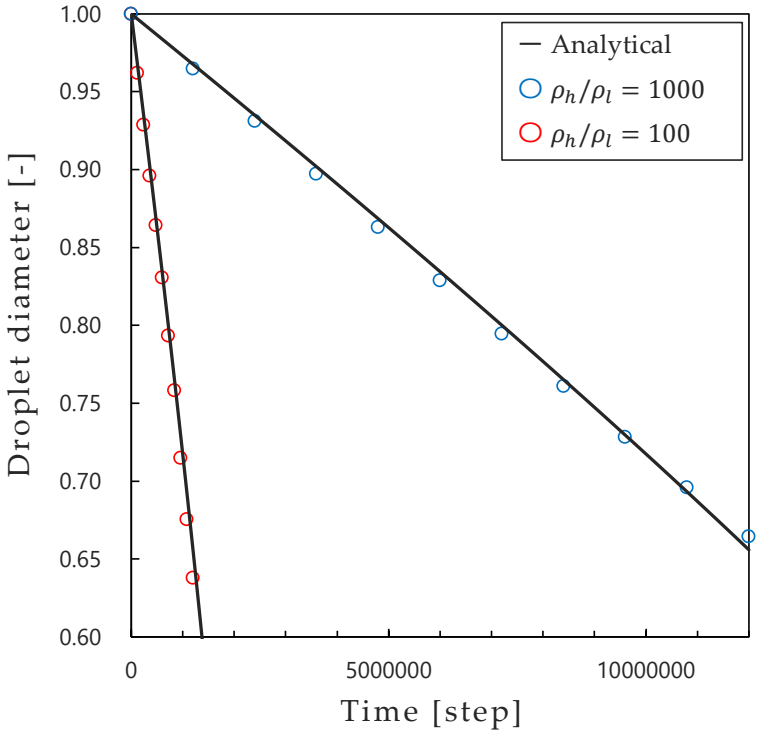

Fig. 4 Evolution of the droplet diameter during evaporation. The lines indicate analytical solutions by Eq. (36) and the dots indicate present numerical results for each density ratio.

3.3 Film boiling

The film boiling[3] is simulated as a phenomenon in which the interface shape changes significantly. Fig. 5 shows the computational model. As an initial condition, a thin vapor phase is placed above the heating wall at temperature T_w which is slightly higher than the saturation temperature, and a liquid phase at the saturation temperature T_{sat} is placed above it. In this situation, the liquid changes to vapor near the heating wall, and vapor region increases. Moreover, the gravity and density differences cause the Rayleigh-Taylor instability. These cause the release of bubbles from near the heating wall. This phenomenon is simulated by the present method. At the outlet boundary, the temperature is given as T_w, the pressure is given as zero, and the normal gradients of velocities and order parameter are given as zero. The body force $F_\alpha^b = (0, (\rho_h - \rho) g_y)$ is applied to the fluids. Table 3 shows the computational conditions. Two cases are simulated, Case1 and Case2. Case1 is a condition that is often used as a benchmark problem. Case2 is a high density ratio condition assuming water-water vapor. However, the surface tension coefficient is set smaller than the real value to avoid turbulence flow. The initial interface shape and the container length D are given as following to facilitate bubble detachment, and Grashof number Gr is the dimensionless numbers defined as following:

$$y = \left(4 + \sin\left(\frac{2\pi x}{D}\right)\right)\frac{D}{y_1} \tag{36}$$

$$D = 2\pi\sqrt{\frac{3\sigma}{g_y(\rho_h - \rho_l)}} \tag{37}$$

$$Gr = \frac{\rho_h g_y (\rho_h - \rho_l) D^3}{\mu_h^2} \tag{38}$$

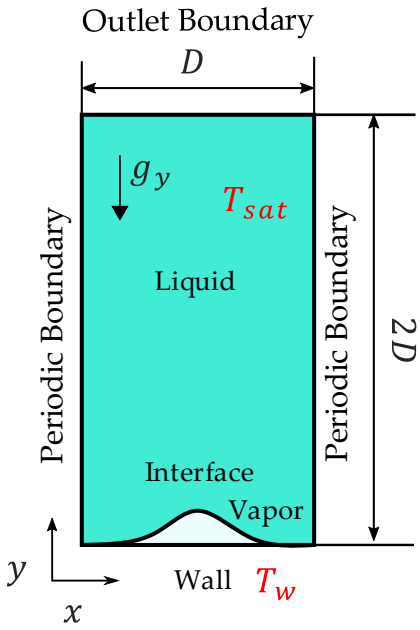

Fig. 5 Computational model for Film boiling

Table 3 Computational conditions for Film boiling

Parameter	Symbol	Case1	Case2
Density ratio	ρ_h/ρ_l	40	1600
Viscosity ratio	μ_h/μ_l	20	25
Specific heat ratio	c_{ph}/c_{pl}	2.0	2.0
Thermal conductivity ratio	λ_h/λ_l	40	25
Stefan number	St	0.2	0.01
Grashof number	Gr	18635	1.0×10^5
Prandtl number	Pr	1.0	2.0
Grids	$D \times 2D$	128×256	128×256
Amplitude coefficient	y_1	128	32

Fig. 6 shows the visualization results of the evolution of liquid-vapor interface of Case1 by present method and Level-Set method as reference[3]. The results show that the phase change occurs near the heating wall, the gas phase region increases, the Rayleigh-Taylor instability is enhanced, the gas phase region rises, and bubble detachment occurs. In this process, the interface profile is almost same as reference, but there are little gaps. When the bubble rise problem without phase change is simulated by Phase Field method and Level-Set method respectively and compared[25,26], there are also little gaps. Therefore, the gaps in this study are within a valid range. Fig. 7 shows the visualization results of the evolution of the interface profile and temperature field of Case2. The results show that film boiling can be simulated even at high density ratios by the present method.

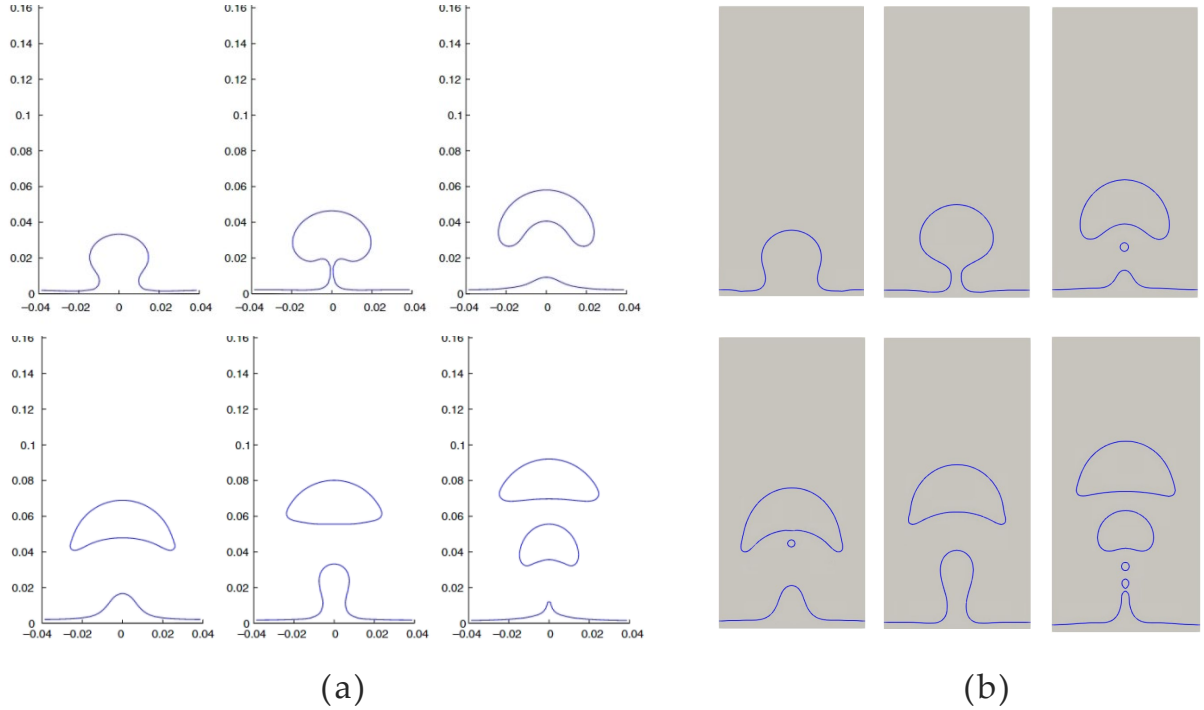

Fig. 6 Evolution of the liquid-vapor interface for Case1. The blue line indicates liquid-vapor interface at $\phi = 0.5$. (a) indicates reference result by Level-Set method[3]. (b) indicates present result.

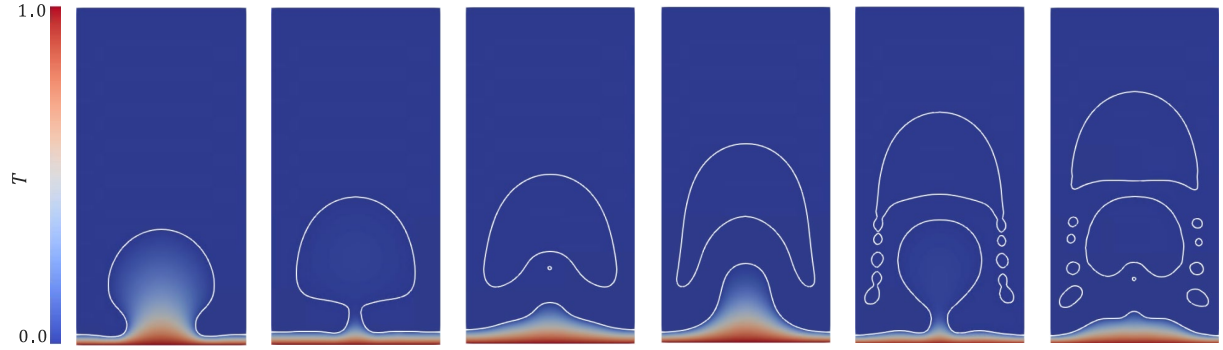

Fig. 7 Evolution of the liquid-vapor interface for Case2. The white line indicates liquid-vapor interface at $\phi = 0.5$ and color indicates temperature. The temperature is made dimensionless as $T = (T^* - T_{sat})/(T_w - T_{sat})$ where T^* is the dimensional temperature.

4. Conclusions

In this study, the velocity-based Phase Field LBM is improved to simulate high density ratio two-phase flows including phase changes with large interface deformations. The macroscopic equations are derived based on the C-A-C equation and the phase change at the interface is modeled as a source term[16]. The LBM is improved by adding forcing terms and the source terms based on the Chapman-Enskog theory to simulate these macroscopic equations. Moreover, in order to improve the numerical stability at high density ratios, the collision term is changed and the method of calculating the gradient of the order parameter is improved. These methods are verified by the Stefan problem, the droplet evaporation problem, and the film boiling problem. These results show that the present method is valid. Moreover, it is shown that the present method can simulate high density ratio two-phase flows including phase changes with large interface deformations.

References

1) S.W.J Welch and J. Wilson: Journal of computational physics, **160**.2 (2000) 662.
2) G. Son, K.D. Vijay, and N. Ramanujapu: Journal of heat transfer, **121**.3 (1999) 623.
3) F. Gibou, L. Chen, D. Nguyen, and S. Banerjee: Journal of Computational Physics, **222**.2 (2007) 536.
4) D. Juric and G. Tryggvason: International journal of multiphase flow, **24**.3 (1998) 387.
5) S. Chen and G. D. Doolen: Annual review of fluid mechanics, **30**.1 (1998) 329.
6) P. Lallemand and L.S. Luo: Physical Review E, **61**.6 (2000) 6546.
7) T. Krüger, H. Kusumaatmaja, A. Kuzmin, O. Shardt, G. Silva, and E. M. Viggen: Springer International Publishing, (2017).
8) X. He, S. Chen, and R. Zhang: Journal of computational physics, **152**.2 (1999) 642.
9) T. Lee and C.-L. Lin: Journal of Computational Physics, **206**.1 (2005) 16.
10) T. Inamuro, T. Ogata, S. Tajima, and N. Konishi: Journal of Computational physics, **198**.2 (2004) 628.
11) L. B. Daniel and K. H. Luo: Physical Review E, **94**.5 (2016) 053313.
12) N. SM. Sheikholeslam, M. T. Rahni, and S. SA. Taleghani: The European Physical Journal Plus, **134**.8 (2019) 1.
13) Y. Q. Zu and S. He: Physical Review E, **87**.4 (2013) 043301.
14) A. Fakhari, T. Mitchell, C. Leonardi, and D. Bolster: Physical Review E, **96**.5 (2017) 053301.
15) Q. Li, K. H. Luo, Q. J. Kang, Y. L. He, Q. Chen, and Q. Liu: Progress in Energy and Combustion Science, **52** (2016) 62.
16) H. Safari, H. R. Mohammad, and K. Manfred: Physical Review E, **88**.1 (2013) 013304.
17) R. H. H. Abadi and H. R. Mohammad: International Journal of Heat and Mass Transfer **127** (2018) 704.
18) R. H. H. Abadi, A. Fakhari, and H. R. Mohammad: Journal of Computational Physics **432**.1 (2021) 110111.
19) Y. Sun and C. Beckermann: Journal of Computational Physics, **220**.2 (2007) 626.
20) P. H. Chiu and Y. T. Lin: Journal of Computational Physics, **230**.1 (2011) 185.
21) M. Geier, A. Fakhari, and T. Lee: Physical Review E, **91**.6 (2015) 063309.
22) W. Li, D. Liu, M. Desbrun, J. Huang, and X. Liu: IEEE transactions on visualization and computer graphics, **27**.7 (2020) 3318.
23) A. Kumar: Journal of Computational Physics, **201**.1 (2004) 109.
24) M. Irfan and M. Muradoglu: Journal of Computational Physics, **337**.15 (2017) 132.
25) Y. P. Sitompul and T. Aoki: Journal of Computational Physics, **390**.1 (2019) 93.
26) M. Kojima and T. Tagawa: International Journal of Microgravity Science and Application, **38**.2 (2021) 380202.